Journal of ELECTRONIC MATERIALS, Vol. 43, No. 4, 2014
DOI: 10.1007/s11664-013-2890-7
© 2013 TMS

Molecular Beam Epitaxial Growth and Properties of Bi_2Se_3 Topological Insulator Layers on Different Substrate Surfaces

ZHIYI CHEN,[1,2,3] THOR AXTMANN GARCIA,[1] JOEL DE JESUS,[1] LUKAS ZHAO,[1] HAIMING DENG,[1] JEFF SECOR,[1] MILAN BEGLIARBEKOV,[1] LIA KRUSIN-ELBAUM,[1] and MARIA C. TAMARGO[1]

1.—The City College of New York, New York, NY, USA. 2.—e-mail: czy1106@gmail.com. 3.—e-mail: zchen2@ccny.cuny.edu

Growth of high-quality Bi_2Se_3 films is crucial not only for study of topological insulators but also for manufacture of technologically important materials. We report a study of the heteroepitaxy of single-crystal Bi_2Se_3 thin films grown on GaAs and InP substrates by use of molecular beam epitaxy. Surface topography, crystal structure, and electrical transport properties of these Bi_2Se_3 epitaxial films are indicative of highly *c*-axis oriented films with atomically sharp interfaces.

Key words: TI, MBE, Bi_2Se_3

INTRODUCTION

Topological insulators (TIs) are a newly discovered class of materials that host new phases of quantum matter in which time-reversal-symmetry-protected electrical conduction is confined to the surfaces and edges.[1–3] In TIs, the spin of charge carriers is locked to their momentum, enabling spatial separation of spin-up and spin-down surface conduction channels. The spin-momentum locking and helical spin textures have been confirmed by angular resolved photoemission spectroscopy (ARPES). [4–6] These properties render TIs ideal candidates for electrical control of spin and for novel spintronic devices.[7,8] Among all three-dimensional (3D) TIs, for example $Bi_{1-x}Sb_x$, Bi_2Se_3, Bi_2Te_3 and Sb_2Te_3, Bi_2Se_3 has the largest band gap (~0.3 eV) and the most ideal single Dirac cone in the middle of the bulk band gap, as is apparent from APRES experiments. However, for bulk grown Bi_2Se_3 and other 3D TIs, the Fermi energy is high in the bulk conduction band and not in the gap.[9] Intermixing of the surface and bulk states at the Fermi energy complicates access to low-energy (Dirac point) charge transport. From the perspective of transport experiments (and device physics), major challenges are significant bulk conduction and the difficulty of separating the surface contribution from that of the bulk.

To address these issues much effort has been devoted to growing epitaxial thin films by molecular beam epitaxy (MBE). Epitaxial layer-by-layer growth by MBE enables precise control over layer thickness, and layers with good uniformity and surface quality are obtained. The slow growth rates and low growth temperatures of MBE furnish highly ordered materials and multilayered structures of dissimilar materials, of importance for the design of devices. The ultra-high vacuum in MBE reduces the incorporation of unwanted impurities, which is crucial to investigation of transport properties, and reduces ambiguities when incorporating wanted dopants.[10] Because these are epitaxial layers, choice of the substrate may be important, and may affect the properties of the materials, for example interface flatness and sample crystallinity. In this work we used a multiple chamber MBE system with III–V and II–VI chambers, which enables sophisticated substrate preparation. Previously, MBE films of Bi_2Se_3 have been grown on such substrates as graphene/SiC,[11–13] silicon,[14–17] $SrTiO_3$,[18,19] GaAs,[20,21] and sapphire[22]. In this study, we investigated Bi_2Se_3 growth on sapphire(001), GaAs(111)B, InP(001), and InP(111)B. GaAs and InP

(Received August 8, 2013; accepted October 25, 2013; published online November 20, 2013)

are two very commonly used III–V semiconductors. Improving sample quality on these two substrates will not only lead to further studies and spintronics applications, but also make the whole family of III–V semiconductors available for growth of Bi_2Se_3 superlattice and heterostructures for device applications.

EXPERIMENTAL PROCEDURES

Our Bi_2Se_3 thin films were grown in a dedicated growth chamber connected by UHV transfer modules to two other chambers, one for growth of II–VI compound semiconductor structures the other for III–V compound structures, so that seamless transfers between chambers can be accomplished, both for use of the diagnostics tools installed in those chambers, for example reflection high-energy-electron diffraction (RHEED), and for growth of multilayered structures combining TIs with conventional semiconductors or metals. The TI chamber is pumped by means of a cryopump and a small ion pump; the vacuum is typically less than 1×10^{-9} Torr during growth. High-purity 6N bismuth (Bi) and selenium (Se) fluxes were provided by conventional Knudsen cells and measured by use of ion gauges placed in the path of the fluxes. We found that an optimum beam equivalent pressure ratio of ~1:10 Bi to Se[10] leads to growth rates of 30 nm/h as confirmed by ex situ film thickness measurement. A lower Bi flux leads to lower growth rates and a higher Bi flux to diminished material quality. Substrate temperature during MBE growth was calibrated to a nominal temperature of 200°C. This condition was optimum; higher temperatures led to reduced growth rate or no growth at all whereas lower temperatures led to diminished material quality. Samples were investigated with RHEED immediately after growth. X-ray diffraction (XRD), atomic force microscopy (AFM), cross-sectional high-resolution transmission electron microscopy (HRTEM), and Raman spectroscopy were performed after removal of the sample from the chamber. Transport measurements were performed in a physical property measurement system (PPMS).

RESULT AND DISCUSSION

Different substrates were used, and different surface-preparation procedures were used for the different substrates. For Bi_2Se_3 grown on GaAs and InP, after use of a standard procedure to remove the oxide, a III–V buffer layer was grown in a III–V chamber before growth of the Bi_2Se_3 layer. GaAs was grown on the GaAs substrate and lattice-matched InGaAs was grown on the InP substrate. For samples grown on InP(001) substrates, a second buffer layer of ZnCdSe, also lattice-matched to InP, was grown on the InGaAs layer in a II–VI chamber, before growth of Bi_2Se_3, which was performed in a third chamber dedicated to growth of this material. For Bi_2Se_3 grown on sapphire, the substrate was heated to 650°C for 2 h before growth. The GaAs and InP substrates used in this experiment were semi-insulating, and the sapphire was undoped. All substrates had a miscut to their desired plane below 0.5°C.

Bi_2Se_3 on Sapphire

Sapphire(0001) was used first because it is relatively well studied[22,23] and it enabled us to verify our Bi_2Se_3 growth conditions. Before growth, sapphire was degassed at 450°C for 30 min, heated to 650°C at 5°/min, then maintained at this temperature for 2 h. Figure 1a shows the RHEED pattern of one sample grown at 200°C with selenium-rich growth conditions (Bi/Se flux ratio approx. 1:10). Sharp 1 × 1 diffraction streaks confirm the good crystalline quality of the film. The crystalline order of the sample was also confirmed by the strong signal from the Bi_2Se_3 layer in XRD (Fig. 1b). The morphology of the films, as characterized by AFM, is shown in Fig. 1c; the RMS roughness was ~0.6 nm. These results are comparable with those reported in the literature for other samples,[22] indicating that our growth conditions are optimum.

Bi_2Se_3 on GaAs(111)B

The main purpose of this work was to grow TI films on III–V semiconducting substrates, because

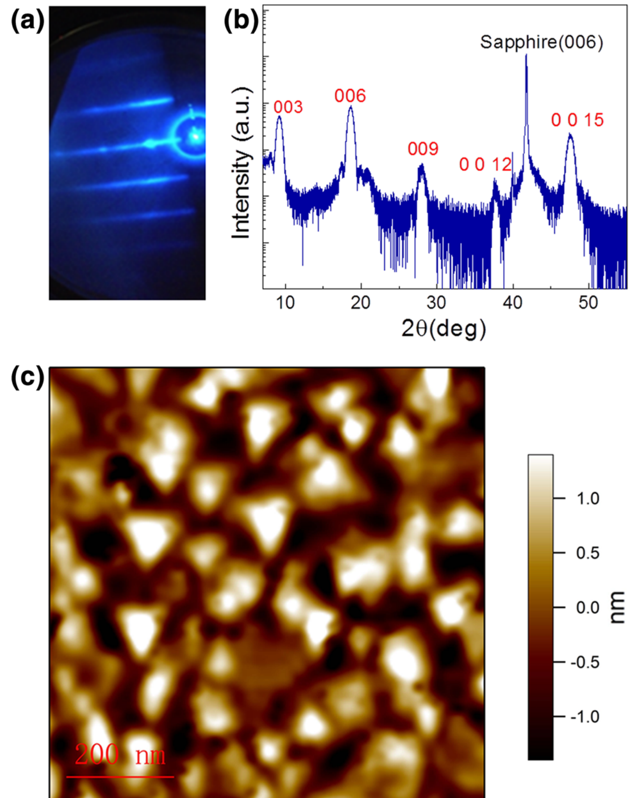

Fig. 1. (**a**) RHEED diffraction patterns of Bi_2Se_3 film on sapphire. (**b**) X-ray diffraction by a ~20 nm thick Bi_2Se_3 film. The (003) family of peaks shows the film is highly *c*-axis oriented. (**c**) AFM image of the surface of the film. The RMS roughness of the film is ~0.6 nm.

of their many technological applications. GaAs(111) is a widely used, technologically important, III–V substrate which has been successfully used with different methods.[20], [21]. The surface has a hexagonal lattice with 3.55% lattice mismatch to Bi_2Se_3. Figure 2a shows the structure of our sample on GaAs(111)B, which includes a 150 nm thick GaAs epitaxial buffer layer. The XRD results in Fig. 2b

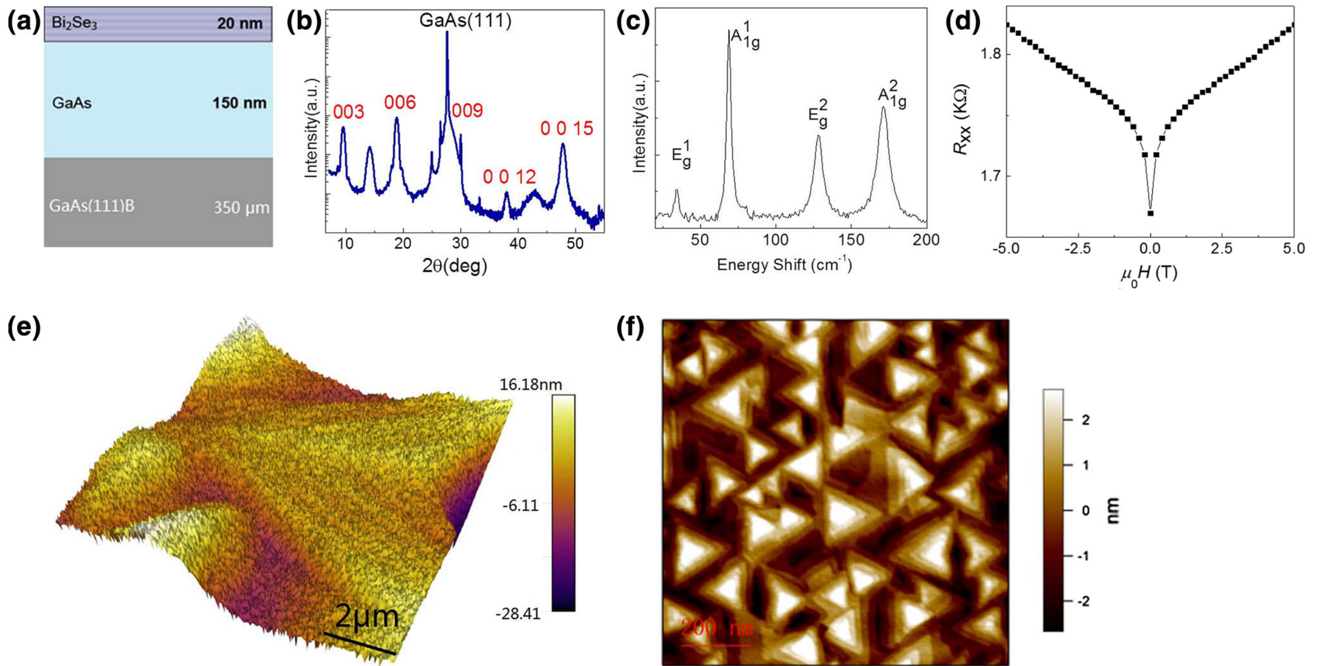

Fig. 2. (**a**) Illustration of the structure grown on GaAs(111)B. (**b**) X-ray diffraction of a ~20 nm thick Bi_2Se_3 film. The (003) family of peaks shows the film is highly *c*-axis orientated. (**c**) Raman spectrum of a 20 nm film shows four characteristic peaks, which are E_g^1, A_{1g}^1, E_g^2 and A_{1g}^2 modes of the Bi_2Se_3 single crystal. (**d**) MR of the sample taken at $T = 2$ K. (**e**) AFM 3D plot of the film showing triangular features. (**f**) AFM image of the surface of a film. The RMS roughness of the film is ~2.6 nm.

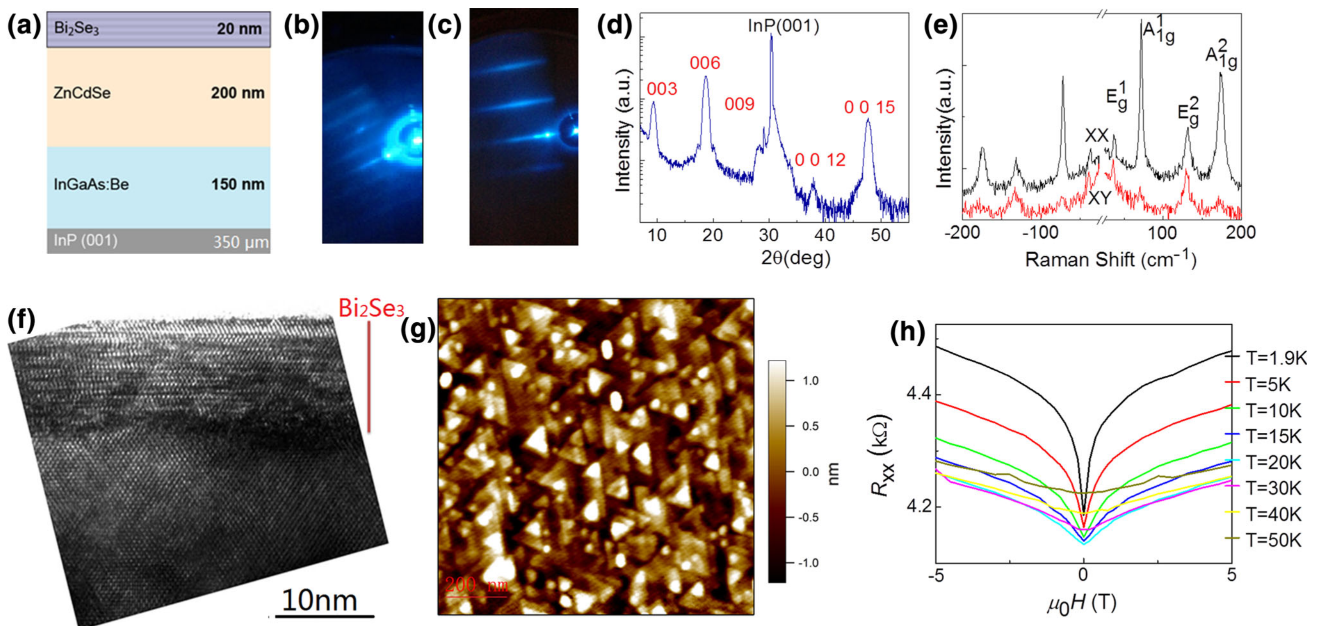

Fig. 3. (**a**) Illustration of the structure grown on InP(001). (**b**) RHEED image of the sample after growth of the ZnCdSe buffer. (**c**) RHEED image of the sample after growth of the Bi_2Se_3 film. (**d**) X-ray diffraction of the Bi_2Se_3 film. (**e**) Raman spectrum with (*XX*) and (*XY*) polarization, collected from the 20 nm Bi_2Se_3 film. (**f**) HRTEM image of the heterostructure showing epitaxial growth of Bi_2Se_3 on ZnCdSe buffer with a clean interface. (**g**) AFM image of the surface of a Bi_2Se_3 film grown on InP(001). The RMS roughness of this film is ~0.8 nm. (**h**) MR data at different temperatures for a sample grown on InP(001), with the thickness $t = 20$ nm.

confirm the crystal structure of the sample. The Raman spectrum of the sample, shown in Fig. 2c, contains four characteristic peaks, at 37 cm^{-1}, 72.5 cm^{-1}, 132 cm^{-1}, and 173.5 cm^{-1} which correspond to the E_g^1, A_{1g}^1, E_g^2 and A_{1g}^2 vibration modes, respectively, as reported for Bi_2Se_3 single crystal.[24] This indicates we have the appropriate modes at the expected energies for Bi_2Se_3. Figure 2e is a 3D plot of the sample's surface obtained by AFM. It shows the presence of triangular features approximately 5 μm × 5 μm in area and 20 nm high. In Fig. 2f, a AFM image of the same sample shows smaller triangular features with a lateral size of approximately 100 nm and a few nanometers high that grew on top of the larger features. Here, the measured RMS was approximately 2.6 nm. Electrical measurements were conducted at T = 2 K by using the van der Pauw contact configuration in magnetic fields up to 5 T applied in the direction perpendicular to the film's plane. Figure 2d shows a cusp in the magnetoresistance (MR) measurement consistent with weak anti-localization, as reported in the literature[30,31] for Bi_2Se_3. From the Hall measurements, our sample was found to be n-type. The sheet carrier concentration was approximately 4×10^{13} cm^{-2} and the mobility was 520 cm^2 $(Vs)^{-1}$ which is comparable with that of samples grown on GaAs by other groups[20]

Bi_2Se_3 on InP(001)

InP is another important III–V substrate with the same zinc blende lattice structure as GaAs. Bi_2Se_3 on InP(001) has been successfully grown by MBE, furnishing Bi_2Se_3 (221),[26] and by hot-well epitaxy[27] furnishing the (001) orientation. In this case we grew a ZnCdSe buffer to improve the chemical compatibility between the substrate and the TI, on the basis of similar work which used a ZnSe buffer on GaAs(111)B.[20] The structure is shown in Fig. 3a. We observed an abrupt transition of the RHEED pattern from the 2 × 1 of the ZnCdSe surface (Fig. 3b) to the sharp and streaky pattern of the Bi_2Se_3 surface (Fig. 3c). When we studied the RHEED screen while rotating the sample, we saw the features in Fig. 3c repeat every 60°, which suggests our samples have a sixfold pattern, which is characteristic of the Bi_2Se_3 hexagonal structure. We also observed a strong signal in XRD from our Bi_2Se_3 layer, as can be seen in Fig. 3d. For Raman spectroscopy (Fig. 3e) we used parallel (*XX*) and perpendicular (*XY*) polarization configurations of the incident and scattered light. For the upper curve, polarization of the incident and scattered light beams was parallel, so the curve corresponds to the $x-x$ component of the Raman tensors. For the lower curve the incident and scattered light beams were polarized perpendicular to each other, so the curve thus represents the $x-y$ component. These results are consistent with the crystal symmetry predicted from group theory.[25]

To confirm epitaxial growth of our Bi_2Se_3 film, HRTEM was performed on one of the samples grown on the ZnCdSe buffer. Figure 3f shows the image of the interface between Bi_2Se_3 and ZnCdSe. It shows a smooth and abrupt interface and good crystalline quality. The surface topography of the samples was also characterized by AFM. Figure 3g shows a typical AFM image of the samples with RMS roughness of ~0.8 nm. A higher-magnification view of the surface revealed triangular terraces on the sample.

To obtain Hall measurements, and to isolate the highly conducting InGaAs buffer, we doped the InGaAs buffer layer with beryllium, which makes the buffer layer p-type, thus creating a space charge region that isolates the TI layer from the buffer layer. Hall measurement shows that the film is n-type, and sheet carrier concentration of the samples are 6–9 × 10^{12} cm^{-2} with mobility of 490–750 $cm^2(V\ s)^{-1}$, comparable with the best reported results for Bi_2Se_3 MBE samples on any substrate.[18,32] Figure 3h shows MR data obtained at different temperatures. With increasing temperature, linear behavior is initially observed at approximately 30 K; eventually a conventional quadratic MR is recovered.

Bi_2Se_3 on InP(111)B

The InP(111) surface is highly interesting because of its very small lattice mismatch (~0.2%) with Bi_2Se_3 and correct symmetry.[28,29] The structure of

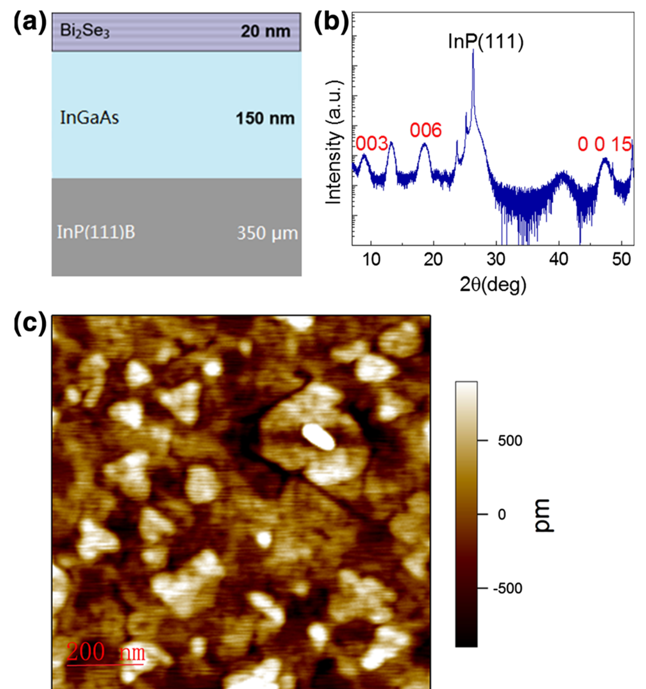

Fig. 4. (**a**) Illustration of the structure grown on InP(111)B. (**b**) X-ray diffraction of the Bi_2Se_3 film. (**c**) AFM image of the surface of a Bi_2Se_3 film grown on InP(111)B. The RMS toughness of this film is ~0.3 nm.

the TI film grown on InP(111)B is shown in Fig. 4a. The sharp and streaky RHEED pattern observed at the end of growth indicates good surface quality. A strong signal from Bi_2Se_3 was also observed in XRD (Fig. 4b). The AFM image in Fig. 4c shows the smoothest surface of any of the substrates we prepared; the RMS roughness, without any ZnCdSe buffer layer, was ~0.3 nm. Other measurements of this sample, including electronic transport are in progress.

CONCLUSIONS

By using III–V and II–VI buffer layers in a multichamber MBE system we were able to grow high-quality Bi_2Se_3 epitaxial layers on III–V semiconductor substrates prepared by use of different surface methods. We obtained good TI quality for GaAs(111)B with GaAs buffer, as reported elsewhere.[20,21] High quality Bi_2Se_3 on InP(001) was obtained by use of a ZnCdSe buffer layer; low carrier concentrations and good carrier mobility were also observed. The best surface-quality film was achieved on InP(111)B substrate, and was grown without a II–VI buffer layer.

ACKNOWLEDGEMENTS

This work was supported by the NSF DMR-1122594 and by NSF CREST Center (CENSES).

REFERENCES

1. L. Fu, C.L. Kane, and E.J. Mele, *Phys. Rev. Lett*. 98, 106803 (2007).
2. X.-L. Qi, T.L. Hughes, and S.-C. Zhang, *Phys. Rev. B* 78, 195424 (2008).
3. H. Zhang, C.-X. Liu, X.-L. Qi, X. Dai, Z. Fang, and S.-C. Zhang, *Nat. Phys*. 5, 438 (2009).
4. Y. Xia, D. Qian, D. Hsieh, L. Wray, A. Pal, H. Lin, A. Bansil, D. Grauer, Y.S. Hor, R.J. Cava, and M.Z. Hasan, *Nat. Phys.* 5, 398 (2009).
5. Y.L. Chen, J.G. Analytis, J.-H. Chu, Z.K. Liu, S.-K. Mo, X.L. Qi, H.J. Zhang, D.H. Lu, X. Dai, Z. Fang, S.C. Zhang, I.R. Fisher, Z. Hussain, and Z.-X. Shen, *Science* 325, 178 (2009).
6. D. Hsieh, Y. Xia, D. Qian, L. Wray, J.H. Dil, F. Meier, J. Osterwalder, L. Patthey, J.G. Checkelsky, N.P. Ong, A.V. Fedorov, H. Lin, A. Bansil, D. Grauer, Y.S. Hor, R.J. Cava, and M.Z. Hasan, *Nature* 460, 1101 (2009).
7. S.-C. Zhang, *Physics* 1, 6 (2008).
8. D. Hsieh, Y. Xia, D. Qian, L. Wray, J.H. Dil, F. Meier, J. Osterwalder, L. Patthey, J.G. Checkelsky, N.P. Ong, A.V. Fedorov, H. Lin, A. Bansil, D. Grauer, Y.S. Hor, R.J. Cava, and M.Z. Hasan, *Nature* 460, 1101 (2009).
9. M.Z. Hasan, and C.L. Kane, *Rev. Mod. Phys*. 82, 3045 (2010).
10. X. Chen, X.C. Ma, K. He, J.F. Jia, and Q.K. Xue,*Adv. Mater*. 23, 1162 (2011).
11. K. He, Y. Zhang, C.Z. Chang, C.L. Song, L.L. Wang, X. Chen, J.F. Jia, Z. Fang, X. Dai, W.Y. Shan, S.Q. Shen, Q. Niu, X.L. Qi, S.-C. Zhang, X.C. Ma, and Q.K. Xue, *Nat. Phys.* 6, 584 (2010).
12. Y. Zhang, C.Z. Chang, K. He, L.L. Wang, X. Chen, J.F. Jia, X.C. Ma, and Q.K. Xue, *Appl. Phys. Lett.* 97, 194102 (2010).
13. C.L. Song, Y.L. Wang, Y.P. Jiang, Y. Zhang, C.Z. Chang, L. Wang, K. He, X. Chen, J.F. Jia, Y. Wang, Z. Fang, X. Dai, X.C. Xie, X.L. Qi, S.-C. Zhang , Q.K. Xue, and X.C. Ma, *Appl. Phys. Lett.* 97, 143118 (2010).
14. G.H. Zhang, H.J. Qin, J. Teng , J.D. Guo, Q. Guo, X. Dai, Z. Fanga, and K.H. Wu, *Appl. Phys. Lett.* 95, 053114 (2009).
15. T. Zhang, P. Cheng, X. Chen, J.-F. Jia, X. Ma, K. He, L. Wang , H. Zhang, X. Dai, Z. Fang, X. Xie, and Q.-K. Xue, *PRL* 103, 266803 (2009).
16. Y.Y. Li, G. Wang, X.G. Zhu, M.H. Liu, C. Ye, X. Chen, Y.Y. Wang, K. He, L.L. Wang, X.C. Ma, H.J. Zhang, X. Dai, Z. Fang, X.C. Xie, Y. Liu, X.L. Qi, J.F. Jia, S.-C. Zhang, and Q.K. Xue, *Adv. Mater.* 22, 4002 (2010).
17. H.D. Li, Z.Y. Wang, X. Kan, X. Guo, H.T. He, Z. Wang, J.N. Wang, T.L. Wong, N. Wang, and M.H. Xie, *New J. Phys.* 12, 103038 (2010).
18. J. Chen, H.J. Qin, F. Yang, J. Liu, T. Guan, F.M. Qu, G.H. Zhang, J.R. Shi, X.C. Xie, C.L. Yang, K.H. Wu, Y.Q. Li, and L. Lu, *Phys. Rev. Lett.* 105, 176602 (2010).
19. G.H. Zhang, H.J. Qin, J. Chen, X.Y. He, L. Lu, Y.Q. Li, and K. H. Wu, *Adv. Funct. Mater.* doi:10.1002/adfm.201002667, (2011).
20. A. Richardella, D.M. Zhang, J.S. Lee, A. Koser, D.W. Rench, A.L. Yeats, B.B. Buckley, D.D. Awschalom, and N. Samarth, *Appl. Phys. Lett.* 97, 262104 (2010).
21. X. Liu, D.J. Smith, J. Fan, Y.-H. Zhang, H. Cao, Y.P. Chen, J. Leiner, B.J. Kirby, M. Dobrowolska, and J.K. Furdyna, *Appl. Phys. Lett.* 171903 (2011).
22. C.Z. Chang, K. He, L.L. Wang, X.C. Ma, M.H. Liu, Z.C. Zhang, X. Chen, Y.Y. Wang, and Q.K. Xue, *SPIN* 1, 21 (2011).
23. M. Liu, C.-Z. Chang, Z. Zhang, Y. Zhang, W. Ruan, K. He, L.L. Wang, X. Chen, J.-F. Jia, S.-C. Zhang, Q. Xue, X. Ma, and Y. Wang, *Phys. Rev. B* 83, 65440 (2011).
24. W. Richter, H. Khler, and C.R. Becker, *Phys. Status Solidi B* 84, 619 (1977).
25. J. Zhang, Z. Peng, A. Soni, Y. Zhao, Y. Xiong, B. Peng, J. Wang, M.S. Dresselhaus, and Q. Xiong, *Nano Lett.* 11, 2407–2414, (2011).
26. Z. Xu, X. Guo, M. Yao, H. He, L. Miao, L. Jiao, H. Liu, J. Wang, D. Qian, J. Jia, W. Ho, and M. Xie, *Adv. Mater.* 25, 1557–1562 (2013).
27. Y. Takagaki, and Jenichen B, *Semicond. Sci. Technol.* 27, 035015 (2012) .
28. X. Guo, Z.J. Xu, H.C. Liu, B. Zhao, X.Q. Dai, H.T. He, J.N. Wang, H.J. Liu , W.K. Ho, and M.H. Xie, *Appl. Phys. Lett.* 102, 151604 (2013).
29. S. Schreyeck, N.V. Tarakina, G. Karczewski, C. Schumacher, T. Borzenko, C. Brunne, H. Buhmann, C. Gould, K. Brunner, and L.W. Molenkamp , *Appl. Phys. Lett.* 102:041914, (2013).
30. J.G. Checkelsky, Y.S. Hor, M.-H Liu., D.-X. Qu, R.J. Cava, and N.P Ong, *Phys. Rev. Lett.* 103, 246601 (2009).
31. H. Peng, K. Lai, D. Kong , S. Meister, Y. Chen, X.-L. Qi, S.-C. Zhang, Z.-X. Shen, and Y. Cui, *Nat. Mater.* 9, 225 (2010).
32. N. Bansal, Y.S. Kim, M. Brahlek, E. Edrey, and S. Oh, *PRL* 109, 116804 (2012).